High frequency piezoresponse force microscopy in the 1-10 MHz regime

K. Seal
The Center for Nanophase Materials Sciences, Oak Ridge National Laboratory, Oak Ridge, Tennessee 37831, USA

S. Jesse and B. J. Rodriguez
Materials Science and Technology Division, Oak Ridge National Laboratory, Oak Ridge, Tennessee 37831, USA

A. P. Baddorf and S. V. Kalinin[a)]
The Center for Nanophase Materials Sciences, Oak Ridge National Laboratory, Oak Ridge, Tennessee 37831, USA

(Received 1 June 2007; accepted 29 October 2007; published online 4 December 2007)

Imaging mechanisms in piezoresponse force microscopy (PFM) in the high frequency regime above the first contact resonance are analyzed. High frequency (HF) imaging enables the effective use of resonance enhancement to amplify weak signals, improves the signal to noise ratio, minimizes the electrostatic contribution to the signal, and improves electrical contact. The limiting factors in HF PFM include inertial stiffening, deteriorating signal transduction, laser spot effects, and the photodetector bandwidth. Analytical expressions for these limits are derived. High-quality PFM operation in the 1–10 MHz frequency range is demonstrated and prospects for imaging in the 10–100 MHz range are discussed. © *2007 American Institute of Physics*.
[DOI: 10.1063/1.2814971]

In the past decade, piezoresponse force microscopy (PFM) has emerged as a key tool for the characterization of electromechanical activity at the nanoscale. In ferroelectric materials, the piezoelectric response is directly related to the primary order parameter, providing an approach for imaging, control, and spectroscopic measurement of local polarization dynamics.[1–3] The ubiquity of piezoelectric coupling in biopolymers[4,5] and III-V nitrides[6] has enabled applications of PFM for high (<10 nm) resolution functional imaging of these materials. With a few notable exceptions,[7,8] operating frequencies in PFM have been limited to 100 kHz, well below the first contact resonance of stiff (>1 N/m) cantilevers. High operation frequencies are expected to provide several advantages, including (a) higher signal to noise ratios due to the larger number of oscillation per pixel time and increased separation from the $1/f$ noise corner (typically ~10 kHz), (b) imaging at cantilever resonances with an associated increase in mechanical amplification of the signal, and (c) inertial stiffening of the cantilever that both minimizes the nonlocal electrostatic force contribution to the signal[9] and improves tip-surface contact. Furthermore, high frequency operation is an essential component of the PFM-based ferroelectric data storage systems, currently limited by the bandwidth of electromechanical detection (1–10 kHz). At the same time, operation at a high mode number can give rise to several problems, including the (a) response averaging due to the finite size of the cantilever beam,[10] (b) loss of sensitivity if the tip-surface spring constant becomes smaller than the effective spring constant of the cantilever,[11] and (c) signal loss due to the bandwidth of the photodetector. Here, we analyze the operation mechanisms in PFM at high frequencies and demonstrate operation at 1–10 MHz.

PFM is based on the detection of mechanical surface deformations induced by a bias, $V_{\mathrm{tip}}=V_{\mathrm{dc}}+V_{\mathrm{ac}}\cos(\omega t)$, applied to a cantilevered atomic force microscope (AFM) tip. The piezoresponse signal measured in PFM is a product of the material's piezoelectric response and the transfer function of the cantilever. The flexural angle of the cantilever due to surface deformation as well as local and nonlocal electrostatic forces is detected by the optical beam deflection technique.[9,11] The resonant frequencies of an AFM cantilever are $\omega_n^2=EI\mu_n^4/mL^4=\mu_n^4k/3mL$, where E is the Young's modulus of the cantilever material, I is the 2nd moment of inertia of the cross section, and m is mass per unit length. The dimensionless wave number μ_n is related to the cantilever spring constant, $k=3EI/L^3$, and tip-surface contact stiffness k_1 as

$$\mu_n=\frac{a_n+b_n\gamma_1}{1+c_n\gamma_1}, \tag{1}$$

where $\gamma_1=k_1/k$ and coefficients a_n, b_n, and c_n for the nth resonance are given in Table I in Ref. 11. The crossover between contact and free cantilever behavior occurs for $\gamma_{1c}(n)=\sqrt{a_n/(b_nc_n)}$ and $\gamma_{1c}(n)\approx\pi^3n^3/4.8$ for $n\geqslant 3$. The minimal contact stiffness of the tip-surface junction in an ambient environment is limited by adhesive and capillary interactions. Estimating $k_1^{\min}\approx 1000$ N/m, the crossover between bound and free behavior corresponds to $n>5.4/k^{1/3}$, where k is in N/m. For stiffer cantilevers, the contact stiffness can be approximated by the Hertzian model as $k_1^H=(6PE^{*2}R_0)^{1/3}$, where E^* is the effective Young's modulus, R_0 is the tip radius of curvature, and $P=kd_0$ is the indentation force, where d_0 is the set-point deflection. This approximation is valid for $k_1^H>k_1^{\min}$. In this case, $n>0.65(d_0R_0E^{*2}/k^2)^{1/9}$ and for typical parameters $R_0=100$ nm, $d_0=300$ nm, $E^*=100$ GPa, and $k=40$ N/m ($k_1^H=1216$ N/m), the crossover occurs for $n>3.85$. For typical operating conditions, the cantilever dynamics are expected to

a)Author to whom correspondence should be addressed. Electronic mail: sergei2@ornl.gov.

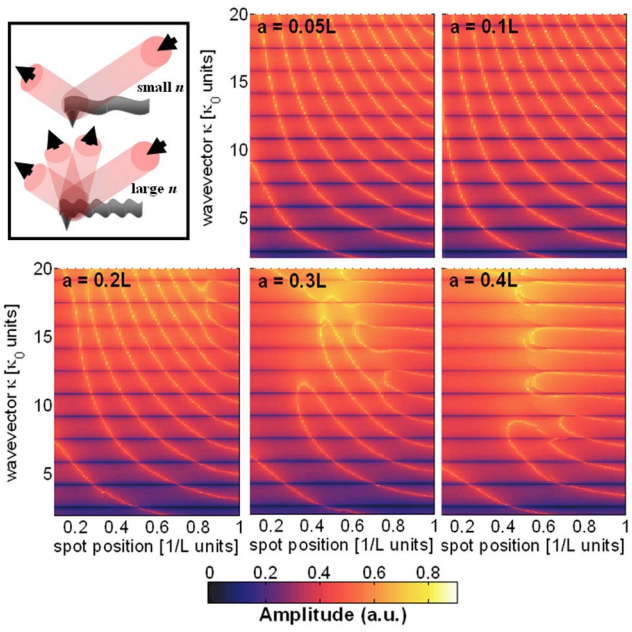

FIG. 1. (Color online) A schematic of the laser spot's effect on the amplitude response. The calculated amplitude response obtained from Eq. (2) for different beam spot sizes a. The amplitude is plotted in normalized arbitrary units as a function of frequency and spot position. L=cantilever length and κ_0 is the first resonance (k_1=100 and k=1 N/m).

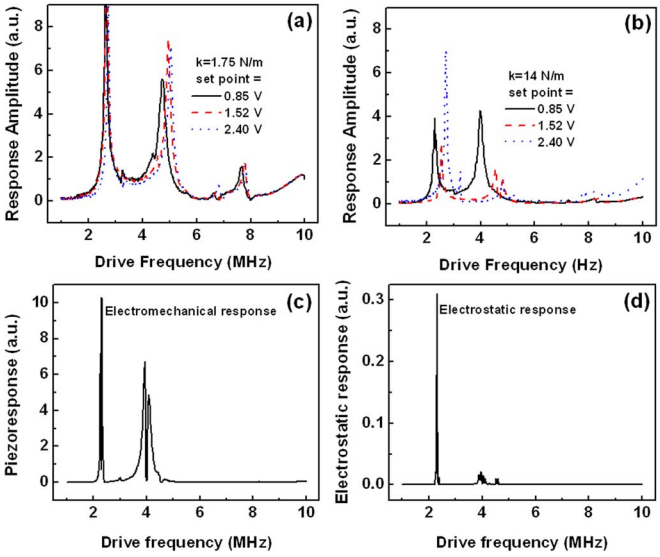

FIG. 2. (Color online) Experimental data from a ceramic PZT sample. The effect of increasing the set point on the frequency dependence of the PFM amplitude for cantilever spring constants (a) k=1.75 N/m and (b) k =14 N/m. The applied bias is 7 V. (c) The piezoresponse extracted from the mixed piezoresponse (PR) signal, PR=$A\cos(\omega t)$. (d) The electrostatic contribution to PR.

be boundlike for the first four resonances, and become progressively free cantileverlike at higher modes. From the analysis above, the crossover from bound to free cantileverlike behavior depends on cantilever parameters primarily through the mode number rather than the cantilever geometry. Although moderate inertial stiffening is beneficial for PFM imaging, operating at very high frequencies (higher modes) leads to signal decay since surface vibrations induced by the piezoeffect are not effectively translated to the cantilever due to inertial stiffening.

The second intrinsic contribution to the PFM response is the laser spot effect. Assuming a Gaussian profile for the laser spot, the response amplitude can be approximated as (assuming that the cantilever is wider than the spot size)

$$P(\omega,x_o) = \int_o^L u'(x,\omega)A(x-x_0)dx, \qquad (2)$$

where L is the length of the cantilever, $u'(x,\omega)$ is the local slope, and $A(x-x_0)$ is the Gaussian function that describes the laser intensity profile. The laser spot size a is defined as the full width at half maximum of the Gaussian function. The effects of the laser spot size and position on the measured response amplitude is calculated from Eq. (2) using cantilever beam profiles derived in Ref. 9 for $k_1 \approx 100$ N/m, as shown in Fig. 1. The laser spot size affects the amplitude of the response for $a \geqslant 2L/n$, where L is the length of the cantilever and n is the mode number. It is thus evident that high-frequency PFM operation requires imaging at lower modes or small spot sizes.

PFM was performed on a commercial Asylum MFP-3D system with an additional lock-in amplifier (Stanford Research Systems SR844) and function generator (SRS DS 345). The Asylum MFP3D was equipped with a fast photodiode (nominal limit 6.25 MHz, corresponding to bandwidth-gain product of 50 MHz and a gain of 8) to enable high frequency measurements. A custom built tip holder allowed direct tip biasing and electrical isolation of the tip in order to avoid capacitive cross-talk with the AFM electronics. Cr–Au coated tips (Micromasch NSC35B and NSC36B) were used to measure the response of a ceramic lead zirconium titanate (PZT) sample in contact mode. An additional LABVIEW interface was used to vary the experimental parameters and collect data. All PFM images were taken at a scan rate of 0.5 Hz.

The frequency dependence of the PFM signal as a function of set-point for different cantilever spring constants is shown in Figs. 2(a) and 2(b). A higher setpoint (i.e., larger indentation force) leads to an increase in the contact resonance frequency. Figure 2(a) indicates that this effect is manifested more strongly for stiffer cantilevers and at higher frequencies. This behavior is in agreement with the analysis above, since for low eigenmodes and soft cantilevers, $\gamma_1 = k_1/k \gg \gamma_c(n)$, and the response is virtually independent of the indentation force. For stiffer cantilevers and higher modes, $\gamma_1 \sim \gamma_c(n)$, and the resonant frequency depends strongly on contact conditions. Finally, for high frequencies and stiff cantilevers, $\gamma_1 \ll \gamma_c(n)$, and the cantilever is essentially free and only weakly affected by surface vibration, resulting in a strong decrease in the response amplitude.

To determine the frequency dependence of the electrostatic and electromechanical contributions to the PFM signal, two-dimensional spectra of the vertical piezoresponse were obtained while varying the dc bias (−4–4 V) and the driving frequency (0.8–10 MHz) with a constant ac bias of 2 V. The frequency dependence of the mixed piezoresponse signal is

$$PR(\omega,V_{\rm dc}) = A\cos\theta = d_1(\omega) + G_{\rm el}(\omega)(V_{\rm dc} - V_{\rm surf}), \qquad (3)$$

where $d_1(\omega)$ and $G_{\rm el}(\omega)$ are the electromechanical and electrostatic contributions. A linear fit of $PR(\omega,V_{\rm dc})$ at each frequency yields $G_{\rm el}(\omega)$ as the slope and $d_1(\omega)$ as the intercept. The results of the deconvolution are shown in Figs. 2(a) and 2(b), respectively. From the magnitudes of the terms, the

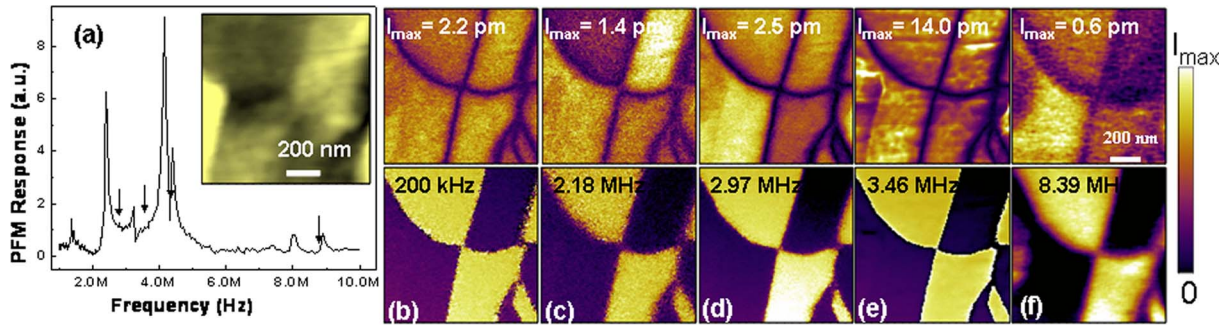

FIG. 3. (Color online) Experimental data from a ceramic PZT sample. (a) The amplitude of the piezoresponse signal at a bias of 7 V showing contact resonances. The inset shows the topography. Also shown are the corresponding images of the PFM amplitude (top row) and phase (bottom row) before (b) 200 kHz and near the contact resonance frequencies (c) 2.18, (d) 2.97, (e) 3.46, and (f) 8.49 MHz.

electromechanical response dominates for tip potentials below 1 V. It is also evident that the electrostatic contribution decreases faster with frequency, favoring a purely electromechanical response at high frequencies.

Finally, to establish the role of frequency on the PFM contrast, imaging was performed at several frequencies. Shown in Fig. 3(a) are the surface topography of a PZT sample and the frequency dependence of the PFM signal for a cantilever with a spring constant $k=14$ N/m. The first contact resonance is clearly seen at 2.18 MHz with higher resonances at 2.96, 3.46, and 8.39 MHz. The corresponding amplitude and phase PFM images both below and above the first resonance, as shown in Figs. 3(b)–3(f), were obtained at a set point of 0.8 V (scan size 1 μm, scan rate 0.5 Hz, and scan direction parallel to cantilever axis). Well demarcated domains are evident in the amplitude images. Clear images are obtained at frequencies as high as 8.4 MHz despite the sharp drop in the photodiode response after 6 MHz. The contrast in the phase images clearly illustrates the reliability of the PFM data. The deflection (d_{max}) values vary due to the use of the contact resonance frequencies. Some amount of topographic cross-talk is evident in Fig. 3(e). The level of noise in the images (which we attribute to thermal noise and topographic cross-talk) was estimated by calculating the variance of the data points from 0.2×0.2 μm^2 areas in two of the domains. The absolute variance from the data was normalized by the average value for comparison. The results shown in Table I illustrate the quality of the images at higher frequencies [the data from Fig. 3(f) are not considered due to the highly reduced contrast]. The disappearance of contrast above ~6 MHz independently of the cantilever type, as confirmed in Fig. 2, is attributed to the photodiode/amplifier bandwidth effect.

TABLE I. Noise estimates for PFM images.

	Noise (σ^2)	
	Amplitude (%)	Phase (degrees)
200 kHz	6.3	6
2.18 MHz	11.2	9.5
2.97 MHz	4.4	5
3.46 MHz	7.6	3.4
8.39 MHz	0.2	2

To summarize, we demonstrate high-veracity PFM imaging in the 1–10 MHz range. The inertial stiffening of the cantilever reduces the electrostatic contribution to the signal and improves the electrical tip-surface contact through effective penetration of the contamination layer. Finally, HF PFM allows resonance enhancement to be used to amplify weak PFM signals. In this regime the response is strongly dependent on the local mechanical contact conditions, and hence an appropriate frequency tracking method is required to avoid PFM-topography cross-talk. The limiting factors for high-frequency PFM, including inertial cantilever stiffening, laser spot effects, and the photodiode bandwidth, are analyzed. Experimentally, the photodiode is shown to be the limiting factor (cutoff at ~6–8 MHz). Inertial stiffening is expected to become a problem for resonances $n>4-5$, independently of cantilever parameters. Finally, the laser beam size becomes a problem for $a\geqslant 2L/n$. These considerations suggest that the use of high-frequency detector electronics, shorter levers with high resonance frequencies, and improved laser focusing will allow the extension of high-frequency PFM imaging to the 10–100 MHz range.

This research was conducted by KS, BJR, and APB at the Center for Nanophase Materials Sciences (data acquisition and analysis) and SJ and SVK at the Materials Science and Technology Division (development of data acquisition software and electronics), Oak Ridge National Laboratory, U.S. Department of Energy.

[1]P. Güthner and K. Dransfeld, Appl. Phys. Lett. **61**, 1137 (1992).
[2]*Nanoscale Characterization of Ferroelectric Materials*, edited by M. Alexe and A. Gruverman (Springer, Heidelberg, 2004).
[3]*Nanoscale Phenomena in Ferroelectric Thin Films*, edited by Seungbum Hong (Kluwer, Dordrecht, 2004).
[4]C. Halperin, S. Mutchnik, A. Agronin, M. Molotskii, P. Urenski, M. Salai, and G. Rosenman, Nano Lett. **4**, 1253 (2004).
[5]S. V. Kalinin, B. J. Rodriguez, S. Jesse, T. Thundat, and A. Gruverman, Appl. Phys. Lett. **87**, 053901 (2005).
[6]B. J. Rodriguez, A. Gruverman, A. I. Kingon, R. J. Nemanich, and O. Ambacher, Appl. Phys. Lett. **80**, 4166 (2002).
[7]C. Harnagea, M. Alexe, D. Hesse, and A. Pignolet, Appl. Phys. Lett. **83**, 338 (2003).
[8]B. D. Huey, in *Nanoscale Phenomena in Ferroelectric Thin Films*, edited by S. Hong (Kluwer, New York, 2004).
[9]S. Jesse, A. P. Baddorf, and S. V. Kalinin, Nanotechnology **17**, 1615 (2006).
[10]T. E. Schäffer, Nanotechnology **16**, 664 (2005).
[11]S. Jesse, B. Mirman, and S. V. Kalinin, Appl. Phys. Lett. **89**, 022906 (2006).